Mirror symmetry breaking with limited enantioselective autocatalysis and temperature gradients: A stability survey

ARTICLE *in* PHYSICAL CHEMISTRY CHEMICAL PHYSICS · DECEMBER 2012

Impact Factor: 4.49 · DOI: 10.1039/c2cp43488a · Source: PubMed

6 AUTHORS, INCLUDING:

Celia Blanco
University of California, Santa Barbara
16 PUBLICATIONS **82** CITATIONS
SEE PROFILE

Josep M. Ribo
University of Barcelona
164 PUBLICATIONS **2,148** CITATIONS
SEE PROFILE

Albert Moyano
University of Barcelona
282 PUBLICATIONS **5,681** CITATIONS
SEE PROFILE

David Hochberg
Instituto Nacional de Técnica Aeroespacial
111 PUBLICATIONS **1,571** CITATIONS
SEE PROFILE

Mirror symmetry breaking with limited enantioselective autocatalysis and temperature gradients: a stability survey

Celia Blanco,[1,*] Josep M. Ribó,[2,3,†] Joaquim Crusats,[2,3,‡] Zoubir El-Hachemi,[2,3,§] Albert Moyano,[2,¶] and David Hochberg[1,**]

[1] *Centro de Astrobiología (CSIC-INTA), Carretera Ajalvir Kilómetro 4, 28850 Torrejón de Ardoz, Madrid, Spain*
[2] *Department of Organic Chemistry, University of Barcelona, c. Martí i Franquès 1, 08028 Barcelona, Catalonia, Spain.*
[3] *Institute of Cosmos Science, University of Barcelona (IEEC-UB), c. Martí i Franquès 1, 08028 Barcelona, Catalonia, Spain.*

We analyze limited enantioselective (LES) autocatalysis in a temperature gradient and with internal flow/recycling of hot and cold material. Microreversibility forbids broken mirror symmetry for LES in the presence of a temperature gradient alone. This symmetry can be broken however when the auto-catalysis and limited enantioselective catalysis are each localized within the regions of low and high temperature, respectively. This scheme has been recently proposed as a plausible model for spontaneous emergence of chirality in abyssal hydrothermal vents. Regions in chemical parameter space are mapped out in which the racemic state is unstable and bifurcates to chiral solutions.

I. INTRODUCTION

Recent experimental reports on the deracemization of racemic mixtures of crystals and on the crystallization from boiling solutions [1–6] are striking examples of novel scenarios for spontaneous mirror symmetry breaking (SMSB) for compounds for which the homochiral interactions are favored over the heterochiral ones. In other words, these are reactions that cannot be explained by Frank-like mechanisms, in which the heterochiral interaction is the favored one. Despite some controversy about the actual mechanisms responsible for the SMSB in these situations, the experimental reports all coincide in that the final state is stationary: mechano-stationary in the case of wet grinding of racemic mixtures of crystals [3–5] and the presence of temperature gradients in the case of deracemization and crystallization in boiling solutions [1, 2]. The above reports stress the fact that the racemic conglomerate crystal mixtures are deracemized in experimental conditions where *chemical equilibrium is not possible*, i.e., they require specific energy input to only some of the species of the system (as in the crystal grinding experiments) or else a non-uniform temperature distribution.

The point of departure for the present paper is: if limited enantioselectivity [7] in experimental conditions of closed systems with a uniform distribution of temperature and energy inexorably yields a final racemic state, [8] then can SMSB occur in scenarios of non-uniform temperature distributions? As it turns out, this is in fact possible in the case that, in addition to a non-uniform temperature distribution, the systems possess a compartmentalization of the enantioselective and the non-enantioselective autocatalyses.

The emergence of chirality in enantioselective autocatalysis for compounds which do not follow Frank-like schemes is investigated here for the limited enantioselectivity (LES) model composed of coupled enantioselective and non-enantioselective autocatalyses. The basic model [7] is defined by the following chemical transformations. Production of chiral compounds L,D from an achiral substrate A:

$$\mathrm{A} \underset{k_{-1}}{\overset{k_1}{\rightleftharpoons}} \mathrm{L}, \qquad \mathrm{A} \underset{k_{-1}}{\overset{k_1}{\rightleftharpoons}} \mathrm{D}. \tag{1}$$

*Electronic address: blancodtc@cab.inta-csic.es
†Electronic address: jmribo@ub.es
‡Electronic address: j.crusats@ub.es
§Electronic address: zelhachemi@ub.es
¶Electronic address: amoyano@ub.es
**Electronic address: hochbergd@cab.inta-csic.es

Autocatalytic production:

$$\mathrm{A} + \mathrm{L} \underset{k_{-2}}{\overset{k_2}{\rightleftharpoons}} \mathrm{L} + \mathrm{L}, \qquad \mathrm{A} + \mathrm{D} \underset{k_{-2}}{\overset{k_2}{\rightleftharpoons}} \mathrm{D} + \mathrm{D}. \tag{2}$$

Limited enantioselectivity:

$$\mathrm{A} + \mathrm{L} \underset{k_{-3}}{\overset{k_3}{\rightleftharpoons}} \mathrm{L} + \mathrm{D}, \qquad \mathrm{A} + \mathrm{D} \underset{k_{-3}}{\overset{k_3}{\rightleftharpoons}} \mathrm{D} + \mathrm{L}. \tag{3}$$

In contrast to the Frank model, LES is able to account for two important facts: namely, (i) the enantioselectivity of any chiral catalyst is limited because of the third reaction Eq.(3), and (ii) the kinetic link between mirror conjugate processes arises from the reversibility of the catalytic stage [7]. The inverse reaction of the non-enantioselective autocatalysis (reaction (3)) substitutes for the mutual inhibition reaction in the Frank model or formation of the heterodimer (L + D → P). Earlier reports had claimed spontaneous mirror symmetry breaking (SMSB) in LES, but this cannot occur in either open or closed systems with a *uniform* temperature distribution. The obstacle comes from microreversibility, where $K(T)$ is the temperature dependent equilibrium constant:

$$\frac{k_i}{k_{-i}} = K(T), \qquad (1 \leq i \leq 3). \tag{4}$$

The condition for the instability of the racemic state is that

$$0 < g < \frac{1-w}{1+3w} < 1, \tag{5}$$

where $g = \frac{k_{-2}}{k_{-3}}$ and $w = \frac{k_3}{k_2}$ [8]. From Eq. (5), we must have $1 - w > 0$ so that $1 > w$. But from Eq. (4), $\frac{k_2}{k_3} = \frac{k_{-2}}{k_{-3}}$, which is incompatible with $1 > w$ and $g < 1$. This is the situation for open systems. For closed systems, it can be shown [8] that the racemic state is unstable provided that

$$0 < g < g_{crit}^{closed} < g_{crit}^{open} = \frac{1-w}{1+3w} < 1, \tag{6}$$

where the critical parameter in a closed system is always bounded above by the corresponding one for open systems, and approaches the latter from below in the limit of large total concentrations C, that is: $g_{crit}^{closed} \to g_{crit}^{open}$. But Eq. (6) is also incompatible with Eq. (4). So the racemic state is always asymptotically stable in this scheme for both open and closed systems held at a uniform temperature. Therefore there can be no asymptotically stable chiral outcome in this model.

Nor can the LES model lead to SMSB in closed systems even with a stationary non-uniform temperature distribution. On the other hand, numerical simulations of chemical kinetics in a two-compartment model [9] demonstrate that SMSB may occur if both catalytic reactions (2) and (3) are spatially separated at different temperatures in different compartments but coupled under the action of a continous internal flow. In such conditions the system can evolve, for certain reaction and system parameters, towards a chiral stationary state, i.e., the system is able to reach a bifurcation point leading to SMSB.

This is an appealing result since numerical simulations using reasonable chemical parameters suggest that an adequate scenario for such an LES-based SMSB would be that of abyssal hydrothermal vents, by virtue of the typical temperature gradients found there and the role of inorganic solids mediating chemical reactions in an enzyme-like role. We therefore proposed [9] that a natural prebiotic scenario for such emergence of chirality is that of abyssal hydrothermal vents and volcanic plumes [10–13] which do have the adequate temperature gradients and contain solids, as for example clays, which have been proposed by several authors [14–18] as catalysts in the prebiotic synthesis of organic compounds.

In view of the above, this paper deals with an analytic/numerical study of the conditions leading to the instability of the ideal racemic composition for the LES model with compartmentalized catalysis (2) and (3) in regions held at different temperatures. The two-compartment model (Sec II) is already sufficiently involved as to make deriving general analytic stability results a near impossible task. We thus focus our efforts on analyzing properties of the racemic fixed point; the analytic conditions for its linear stability can be set up and then tested in numerical domains. The direct study of the stationary chiral solutions is substantially more complicated and algebraically unwieldy. Nevertheless, the characterization of a racemic state as unstable necessarily implies that the system evolves to a state of non-racemic composition. Such a nonracemic state could be stable, chaotic or oscillatory. However, the

many numerical SMSB tests performed for reasonable reaction parameters and under the thermodynamic constraints imposed by the principle of microreversibility and the temperature dependencies of the reaction rate constants (see Sec III) have in all cases led to a stable chiral state. These stable states are scalemic mixtures of enantiomeric excesses (ee) whose values depend on the parameters of the phase diagram. We first review the impossibility of SMSB in LES with a stable temperature gradient. We then prove that SMSB in such a system is possible when the two catalyses (2) and (3) are compartmentalized (localized) in different temperature regions connected by an internal flow of material.

II. LES WITH A TEMPERATURE GRADIENT

Consider the LES scheme in a temperature gradient: this permits the reaction rates to vary spatially in the system, from one place to another, and might provide a way to achieve mirror symmetry breaking. The reverse reaction of (3) in one region (compartment) could be faster that the reverse of (2) in the other. And then mixing could bring the hot and cold material into contact. We model this by a closed two-compartment system with volumes V, V^*; each compartment held at a uniform temperature, $T^* > T$, and internally coupled by a constant internal flow or recycling. The concentrations, and reaction rates for the second compartment are labeled by an asterisk, see Figure 1. We extend the basic LES scheme Eqs.(1,2,3), by including the terms corresponding to the internal flow. The internal

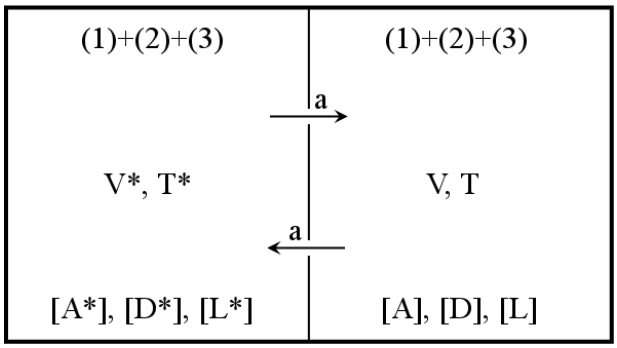

FIG. 1: Limited enantioselectivity (LES) in two compartments with volumns V and V^* each held at different temperatures $T^* > T$ and interconnected by an internal flow a of material. See Ref. [9].

"flow" parameter a has units of volume/time; V and V^* denote the volumes of each compartment. The corresponding rate equations for the two-compartment system have been derived in [9].

A. New variables

For setting up a stability analysis it is convenient to employ the sums and differences of the concentrations $\chi = [L]+[D]$, $y = [L]-[D]$, $\chi^* = [L^*]+[D^*]$ and $y^* = [L^*]-[D^*]$. In terms of these, the rate equations take the following form:

$$\frac{d[A]}{dt} = -2k_1[A] - (k_2[A] + k_3[A] - k_{-1})\chi + \frac{k_{-2}}{2}(y^2+\chi^2) + \frac{k_{-3}}{2}(\chi^2 - y^2) + \frac{a}{V}([A^*] - [A]), \tag{7}$$

$$\frac{d\chi}{dt} = 2k_1[A] + (k_2[A] - k_{-1})\chi + k_3[A]\chi - k_{-2}\frac{(\chi^2+y^2)}{2} - k_{-3}\frac{(\chi^2-y^2)}{2} + \frac{a}{V}(\chi^* - \chi), \tag{8}$$

$$\frac{dy}{dt} = (k_2[A] - k_{-1})y - k_{-2}\chi y - k_3[A]y + \frac{a}{V}(y^* - y), \tag{9}$$

$$\frac{d[A^*]}{dt} = -2k_1^*[A^*] - (k_2^*[A^*] + k_3^*[A^*] - k_{-1}^*)\chi^* + k_{-2}^*(y^{*2}+\chi^{*2}) + \frac{k_{-3}^*}{2}(\chi^{*2} - y^{*2}) + \frac{a}{V^*}([A] - [A^*]), \tag{10}$$

$$\frac{d\chi^*}{dt} = 2k_1^*[A^*] + (k_2^*[A^*] - k_{-1}^*)\chi^* + k_3^*[A^*]\chi^* - k_{-2}^*\frac{(\chi^{*2} + y^{*2})}{2} - k_{-3}^*\frac{(\chi^{*2} - y^{*2})}{2} + \frac{a}{V^*}(\chi - \chi^*), \tag{11}$$

$$\frac{dy^*}{dt} = (k_2^*[A^*] - k_{-1}^*)y^* - k_{-2}^*\chi^* y^* - k_3^*[A^*]y^* + \frac{a}{V^*}(y - y^*). \tag{12}$$

They satisfy the constant mass constraint:

$$V([A] + \chi) + V^*([A^*] + \chi^*) = C, \tag{13}$$

where C is the total conserved mass in the complete two-compartment system.

III. CONSTRAINTS FROM ARRHENIUS-EYRING

Certain thermodynamic relationships hold among the reaction rates in both compartments. These will be used to prove that SMSB is also impossible for the scheme presented in Sec II in a background temperature gradient. Following this demonstration, we then introduce the variant of LES that can and does lead to SMSB.

From Arrhenius-Eyring, the forward (and reverse) reaction rates for reaction i at temperatures T^* and $T < T^*$ are [19]

$$k_i^* = \big(\frac{k_B T^*}{h}\big)\, e^{-\frac{\Delta G_i(T^*)}{RT^*}}, \qquad k_{-i}^* = \big(\frac{k_B T^*}{h}\big)\, e^{-\frac{\Delta G_{-i}(T^*)}{RT^*}}, \tag{14}$$

$$k_i = \big(\frac{k_B T}{h}\big)\, e^{-\frac{\Delta G_i(T)}{RT}}, \qquad k_{-i} = \big(\frac{k_B T}{h}\big)\, e^{-\frac{\Delta G_{-i}(T)}{RT}}, \tag{15}$$

here

$$\Delta G_i(T) = \Delta H_i - T\Delta S_i \tag{16}$$

denotes the difference in free energy between the activated state (transition state) and the reactants, while

$$\Delta G_{-i}(T) = \Delta H_{-i} - T\Delta S_{-i}, \tag{17}$$

is the free energy difference between the activated state (transition state) and the products; H and S denote the enthalpy and entropy, respectively. From the above we can obtain a relation between the forward reaction rates i in each compartment:

$$k_i^* = \big(\frac{T^*}{T}\big)\, \exp\Big(-\frac{\Delta H_i}{R}\big(\frac{1}{T^*} - \frac{1}{T}\big)\Big) k_i. \tag{18}$$

Clearly, once the values of the k_i are chosen for the reference compartment at T, we are not free to *independently* choose the reaction rates k_i^* at the higher temperature T^*.

The fundamental microreversibility condition Eq.(4) together with Arrhenius-Eyring implies

$$\frac{k_i}{k_{-i}} = \frac{e^{-\frac{\Delta G_i}{RT}}}{e^{-\frac{\Delta G_{-i}}{RT}}} = e^{(\Delta G_{-i} - \Delta G_i)/RT} = K(T), \tag{19}$$

$$\Leftrightarrow\ \Delta G_{-i} - \Delta G_i \equiv \Delta\Delta G, \tag{20}$$

that is, the difference of the free energy differences $\Delta\Delta G$ must be *independent* of i, that is, independent of the specific ith reaction. This implies that the individual double differences in enthalpy and in entropy must also be independent of reaction i, so we must also have

$$\Delta\Delta H = (\Delta H_{-i} - \Delta H_i), \tag{21}$$

$$\Delta\Delta S = (\Delta S_{-i} - \Delta S_i). \tag{22}$$

This also gives us an expression for calculating K:

$$K(T) = e^{\frac{\Delta\Delta H}{RT}} e^{-\frac{\Delta\Delta S}{R}}. \tag{23}$$

The inverse reaction rates are obtained through the constraint Eq.(4) as follows:

$$k_{-i} = \frac{k_i}{K(T)}. \tag{24}$$

We also note that if the constraint Eq. (4) is satisfied at one specific temperature T, then it will automatically hold at all others, that is

$$\frac{k_i^*}{k_{-i}^*} = K(T^*) = e^{\frac{\Delta\Delta H}{RT^*}} e^{-\frac{\Delta\Delta S}{R}}, \qquad (1 \leq i \leq 3). \tag{25}$$

The ratio of the equilibrium constants is given by

$$\frac{K(T^*)}{K(T)} = \exp\Big(\frac{\Delta\Delta H}{R}(\frac{1}{T^*} - \frac{1}{T})\Big). \tag{26}$$

The algebraic intricacy of the model in Sec II is already such that we are unable to obtain *useful* and manageable analytic closed form expressions for the conditions leading to the instability of the racemic solution. The situation is even worse for obtaining analytic information regarding the possible stationary chiral solutions. We appeal instead to chemically inspired conjectures that can be tested numerically for coherence and compatibility with microreversibility.

First, it is clear that in view of the gradient $T < T^*$, the putative condition, which could conceivably lead to symmetry breaking in the limit of small values of a,

$$\begin{array}{cccccc} & k_{-2} < k_{-3} & \& & k_2 > k_3 & \text{at} & T \\ \text{and} & k_{-2}^* < k_{-3}^* & \& & k_2^* > k_3^* & \text{at} & T^*, \end{array} \tag{27}$$

is incompatible with the constraints in Eqs. (23,25). This condition (27) is inspired by the observation that for $a \to 0$, the two compartments are practically isolated from each other and can be treated as approximately independent. These are thus the necessary conditions for obtaining an unstable racemic solution in each compartment (see Sec I). But they are incompatible with microreversibility.

Secondly, the analysis in Sec I suggests that SMSB might occur when the inverse reaction of (3) in one region is *faster* than the inverse reaction of (2) in the other region. Taking microreversibility into account, the only way this might be achieved is, for example, by arranging for

$$\begin{array}{cccccc} & k_{-3} < k_{-2} & \& & k_2 > k_3 & \text{at} & T \\ \text{and} & k_{-2}^* < k_{-3}^* & \& & k_2^* < k_3^* & \text{at} & T^*. \end{array} \tag{28}$$

But this is forbidden by virtue of Eq. (26), which is satisfied by the ratio of the equilibrium constants. So a temperature gradient and internal flow are by themselves, not enough to produce a bifurcation. Actually, no spatially varying temperature profile is sufficient, as can be seen by partitioning the closed system into a number of sufficiently small regions within which the local temperature is approximately uniform.

IV. TEMPERATURE GRADIENT AND IMMOBILIZED CATALYSTS

Our working hypothesis is that a *necessary but not sufficient* condition for the instability of the racemic solution is $k_{-3}^* > k_{-2}$ and $k_2 > k_3^*$ in the presence of immobilized catalysts that ensure that $k_{\pm 2}^* = 0$ in one region and $k_{\pm 3} = 0$ in the other [9]. Other conditions (total system concentration C, the flow rate a, compartment volumes V, V^*, etc.) also come into play for determining the overall instability, in a highly nontrivial and nonlinear fashion.

$$A = \begin{pmatrix} (-2k_1 - [k_2+k_3]\bar{\chi} - \frac{a}{V} - \frac{a}{V^*}) & (-(k_2+k_3)\bar{A} + (k_{-2}+k_{-3})\bar{\chi} + k_{-1} - \frac{a}{V^*}) & -\frac{a}{V} \\ (2k_1 + [k_2+k_3]\bar{\chi}) & ((k_2+k_3)\bar{A} - k_{-1} - (k_{-2}+k_{-3})\bar{\chi} - \frac{a}{V}) & \frac{a}{V} \\ -\frac{V}{V^*}(2k_1^* + [k_2^*+k_3^*]\bar{\chi}^*) & (\frac{a}{V^*} - \frac{V}{V^*}(2k_1^* + [k_2^*+k_3^*]\bar{\chi}^*) & ([k_2^*+k_3^*](\frac{C}{V^*} - \frac{V}{V^*}(\bar{A}+\bar{\chi}) - \bar{\chi}^*) \\ & & -k_{-1}^* - (k_{-2}^*+k_{-3}^*)\bar{\chi}^* - \frac{a}{V^*} \\ & & -(2k_1^* + [k_2^*+k_3^*]\bar{\chi}^*)) \end{pmatrix}, \tag{31}$$

$$B = \begin{pmatrix} \Big(-k_{-1} - k_{-2}\bar{\chi} + (k_2 - k_3)\bar{A} - \frac{a}{V} \Big) & \frac{a}{V} \\ \frac{a}{V^*} & \Big((k_2^* - k_3^*)(\frac{C}{V^*} - \frac{V}{V^*}(\bar{A}+\bar{\chi}) - \bar{\chi}^*) - k_{-1}^* - k_{-2}^*\bar{\chi}^* - \frac{a}{V^*} \Big) \end{pmatrix}. \tag{32}$$

A. Linear stability analysis of the stationary racemic fixed point

The equations (9,12) for $\frac{dy}{dt} = \frac{dy^*}{dt} = 0$ are identically satisfied for the stationary solution $\bar{y} = \bar{y}^* = 0$. We therefore carry out a stability analysis of this racemic fixed point and determine whether the racemic solution (racemic in *both* compartments) is asymptotically stable or unstable. This will depend on the internal *flow parameter* a that characterizes the cycling of hot to cold material between the two compartments. Clearly, if we set $a = 0$, we merely recover two isolated copies of LES in independent closed compartments, each one at a constant temperature, and there can be no mirror symmetry breaking in this situation; the considerations of Sec I apply.

An algebraic advantage of studying the racemic fixed point $\bar{y} = \bar{y}^* = 0$ is that the five independent concentration fluctuations decouple into two sets of three and two, respectively. This situation is reflected in the structure of the Jacobian J which then reduces to a block-diagonal form with a 3×3 sub-block corresponding to the fluctuations $(\delta A, \delta\chi, \delta\chi^*)$ and a 2×2 sub-block corresponding to $(\delta y, \delta y^*)$ thus:

$$J = \begin{pmatrix} A^{3\times3} & D^{3\times2} \\ C^{2\times3} & B^{2\times2} \end{pmatrix} \Rightarrow \begin{pmatrix} A^{3\times3} & 0 \\ 0 & B^{2\times2} \end{pmatrix}. \tag{29}$$

The temporal evolution of the linearized concentration fluctuations about the racemic fixed point $\bar{y} = \bar{y}^* = 0$ of the kinetic equations is given by

$$\frac{d}{dt}\begin{pmatrix} \delta A \\ \delta\chi \\ \delta\chi^* \end{pmatrix} = A \begin{pmatrix} \delta A \\ \delta\chi \\ \delta\chi^* \end{pmatrix}$$
$$\text{and} \quad \frac{d}{dt}\begin{pmatrix} \delta y \\ \delta y^* \end{pmatrix} = B \begin{pmatrix} \delta y \\ \delta y^* \end{pmatrix}, \tag{30}$$

where the 3×3 array A is given by Eq. (31) and the 2×2 array B is given by Eq.(32), (see Appendix A)

The Jacobian matrix J (29) must be evaluated on non-negative stationary solutions $\bar{A} \geq 0, \bar{\chi} \geq 0, \bar{\chi}^* \geq 0$ corresponding to $\bar{y} = \bar{y}^* = 0$. Then, to assess the stability of the solution, the five eigenvalues $\lambda_i, i = 1, 2, ..., 5$ of the Jacobian must be calculated. If any one of these five eigenvalues is positive (or their real part, if complex) then the solution is unstable. This means that the system will evolve to a chiral state, so mirror symmetry will be broken. Only if *all* five of the eigenvalues are negative (real part) can we claim that the solution is stable. Deriving manageable and useful closed form expressions for the eigenvalues λ_i of Eqs. (31,32) is practically impossible, due to the fact that the racemic fixed point solutions $\bar{A}, \bar{\chi}, \bar{\chi}^*$ lead to unwieldy expressions (as solutions of coupled quartic equations). On the other hand, direct numeric calculation of the fixed point solutions and their associated eigenvalues is amenable and provides a wealth of information about the dynamic stability of the underlying model, as functions of the chemical rates and the system parameters. We will therefore map out regions of stability/instability in parameter space. We carry this out assuming immobilized catalyst from the start, setting k_2^*, k_{-2}^* to zero in one compartment, and k_3, k_{-3} in the other. Variations in the remaining rate constants are carried out satisfying the constraints in Eqs. (24,25).

We apply a second, independent, stability test which does not require calculating the eigenvalues: namely, the Routh-Hurwitz (RH) criteria. We derive explicit expressions whose algebraic signs indicate whether the racemic fixed point is stable or unstable. The canonical form of the characteristic polynomial for the complete 5×5 jacobian Eq.

(29) is

$$P(\lambda) = \lambda^5 + a_1\lambda^4 + a_2\lambda^3 + a_3\lambda^2 + a_4\lambda + a_5 = 0. \tag{33}$$

Then (see Appendix B of [20]) there are conditions on the coefficients a_i, $i = 1, 2, ..., 5$ such that the zeros of $P(\lambda)$ have $\Re\lambda < 0$. The necessary and sufficient conditions for this to hold are the Routh-Hurwitz conditions. One such form, together with

$$a_5 \equiv -\det\big(B\big)\det\big(A\big) > 0, \tag{34}$$

is that

$$D_1 = a_1 \equiv -[\mathrm{tr}\big(B\big) + \mathrm{tr}\big(A\big)] > 0, \,\& \tag{35}$$
$$D_2 = (a_1a_2 - a_3) > 0, \,\& \tag{36}$$
$$D_3 = a_3D_2 + a_1(a_5 - a_1a_4) > 0, \,\& \tag{37}$$
$$D_4 = a_4D_3 - a_5\{a_1(a_2^2 - a_4) - (a_3a_2 - a_5)\} > 0. \tag{38}$$

The expressions a_i can be read off directly from comparing the polynomial in Eq.(33) to $-P$ calculated in Eq. (B5).

If *any* of the above conditions Eqs. (34-38) does not hold, then the racemic fixed point solution is unstable. As before, this means the system will evolve to a chiral state. This test can be compared with direct numerical calculation of the five eigenvalues λ_i $i = 1, 2, 3, 4, 5$ (the roots of the characteristic polynomial). We find complete agreement between the two methods (eigenvalues, RH criteria) employed. We emphasize that an instability in the racemic fixed point implies the onset of a bifurcation to a non-racemic, hence chiral, solution.

B. Domains of instability

We initiate the procedure outlined above by specifying the forward/reverse reaction rates (temperature differences are treated implicitly), the internal flow rate, the compartment volumes and the conserved total system mass:

$$\{k_{\pm i}(T), k^*_{\pm i}(T^*)\}, a, V, V^*, C, \tag{39}$$

the individual rates of course satisfying microreversibility at the respective temperatures T, T^*. We then solve for the complete racemic fixed point solution, retaining only those solutions that are non-negative:

$$\left\{\frac{dA}{dt} = 0, \frac{d\chi}{dt} = 0, \frac{d\chi^*}{dt} = 0\right\}_{\bar{y}=\bar{y}^*=0} \Rightarrow \{\bar{A}, \bar{\chi}, \bar{\chi}^*\}_{\geq 0}. \tag{40}$$

We next evaluate the Jacobian matrix over this fixed point solution:

$$J \Rightarrow \begin{pmatrix} A^{3\times 3} & 0 \\ 0 & B^{2\times 2} \end{pmatrix}|_{\{\bar{A},\bar{\chi},\bar{\chi}^*\}_{\geq 0}}. \tag{41}$$

As a final step we evaluate the five RH conditions Eqs.(34- 38): are they *all* true or not? If not, then we immediately know that the racemic fixed point is unstable for the parameter choice made in Eq. (39). Hence any fluctuation about the idealized racemic composition will grow and drive the system to a chiral final state. In parallel, we also evaluate numerically the five roots of the characteristic polynomial λ_i $i = 1, 2, 3, 4, 5$ and verify agreement between RH criteria and the eigenvalues. We use the RH criteria to map out the regions of linear instability for the racemic solution.

We start with the reaction rates $k_1 = 10^{-9}$, $k_{-1} = 10^{-15}$, $k^*_1 = 10^{-7}$, $k^*_{-1} = 10^{-11}$, $k_2 = 10^2$, $k_{-2} = 10^{-4}$, $k^*_2 = 0$, $k^*_{-2} = 0$, $k_3 = 0$, $k_{-3} = 0$, $k^*_3 = 10^1$, $k^*_{-3} = 10^{-3}$, the volume and flux parameters $V = 10$, $V^* = 10$, $a = 0.1$, and the initial concentrations $[A]_0 = 10^{-6}$, $[A^*]_0 = 10^{-6}$, $[L]_0 = 10^{-11}$, $[D]_0 = 10^{-11}$, $[L^*]_0 = 10^{-11} + 10^{-21}$, $[D^*]_0 = 10^{-11}$ as employed in Ref [9]. This point in parameter space was shown to lead to SMSB and subsequent chiral amplification from direct numerical integration of the differential rate equations. These specific rate values and system parameters were obtained after performing a set of trial and error numerical simulations obeying the condition $k^*_{-3} > k_{-2}$ and $k_2 > k^*_3$ which corresponds approximately to thermodynamically unattainable conditions for systems with a uniform temperature and lacking compartments. Once obtained, we can exploit the stability analysis to map out and amplify the full domain of instability of the racemic solution.

We consider how the stability of the racemic fixed point responds to variations of selected pairs of variables about this point. In Fig 2 we display the regions of stability/instability as a function of (a) the two compartment volumes

V and V^*, (b) the flow rate a versus equal compartment volumes $V = V^*$, (c) the total concentration C versus flow rate a, and (d) $\alpha = \frac{k^*_{-3}}{k_{-2}}$ versus k_{-2}. The graphs in (a) and (b) merely tell us that the ratio of the compartment volumes cannot be either arbitrarily large nor small, and that for equal compartment volumes, there is a minimum flow rate below which no chiral state can be obtained. Perhaps more surprising are the trends indicated in Fig 2 (c) and (d): for a given flow rate there is a critical system concentration *above* which mirror symmetry cannot be broken and in (d), for a given value of k_{-2} a bounded region in k^*_{-3} in which the racemic state is unstable, and this region narrows down and pinches off for a critical value of k_{-2}. We can here appreciate that the conjecture $k^*_{-3} > k_{-2}$ is necessary, but certainly not sufficient to lead to an instability in the racemic state. We therefore delve further into this nonlinear relationship by considering how the instability varies with k^*_{-3}, k_{-2} and with the flow rate a. In Fig 3 we display a sequence of plots showing how the region of instability grows in area as we scale up the flow rate. For a given flow rate, there is a maximum value of k_{-2} beyond which no value of k^*_{-3} will lead to an instability, and this maximum value scales with a. Below this maximum value, there are always upper and lower bounds on k^*_{-3} between which the system is unstable. These bounds also scale with a. In Fig 3 we keep both k^*_{-3} and k_{-2} fixed and vary a: increased flow enlarges the region of instability. This can also be appreciated in the three-dimensional plot in Fig 4 exhibiting how the region of instability expands in cross sectional area as we scale up the internal flow rate a.

In Fig 5 we display a sequence of plots showing how the region of instability decreases in area as we scale up the total concentration C, over three orders of magnitude. As C is scaled up, the rates k^*_{-3}, k_{-2} decrease in magnitude in such a way as to preserve the *shape* of the region of instability. As before, for a given total concentration, there is a maximum value of k_{-2} beyond which no value of k^*_{-3} will lead to an instability, and this maximum value inversely scales with C. Below this maximum value, there are always upper and lower bounds on k^*_{-3} between which the system is unstable. These bounds also inversely scale with C. A three-dimensional plot in Fig 6 indicates the cross-sectional area of the domain of instability shrinks as we scale up the total system concentration C. Dilute concentrations are more favorable for SMSB [9].

V. SYMMETRY BREAKING AND ENTROPY PRODUCTION

We illustrate the above considerations by way of two examples. The inherent chiral fluctuations about the ideal racemic composition can be modeled by starting with an initial ee below the statistical deviation. In the first simulation, Figure 7, we begin with $[A]_0 = [A^*]_0 = 1 \times 10^{-6}M$, $[L]_0 = [D]_0 = 1 \times 10^{-11}M$, $[L^*]_0 = 1 \times 10^{-6} + 1 \times 10^{-21}M$, and $[D^*]_0 = 1 \times 10^{-6}M$. In the second, Figure 8, we keep the same rates and system parameters but start off with different initial concentrations: $[A]_0 = [A^*]_0 = 1 \times 10^{-11}M$, $[L]_0 = [D]_0 = 5 \times 10^{-7}M$, $[L^*]_0 = 5 \times 10^{-7} + 1 \times 10^{-20}M$, and $[D^*]_0 = 5 \times 10^{-7}M$.

We calculate and superimpose the entropy production[21] σ on the concentration curves. The entropy production is a measure of the dissipation of the out-of-equilibrium process under study. For the initial conditions leading to Figure 7, the entropy production suffers a peak at the onset of the induction period, reflecting the fact that the catalysis of enantiomers Eq. (2), and subsequent depletion of achiral substrate, is the most important contribution. The production then falls to a small but constant nonzero value and remains nonzero as long as the system is kept out of equilibrium. In the case of Figure 8, the entropy production starts off from a large value then drops (at the same time scale as the peak in Figure 7) and subsequently drops down to its minimum nonzero value at the symmetry breaking bifurcation. It again remains small but nonzero as long as the system is kept out of equilibrium.

VI. CONCLUDING REMARKS

Compartmentalization, together with different temperatures for the enantioselective and the non-enantioselective autocatalyses, was shown to be a necessary condition for SMSB. The temperature gradient and internal flow or recycling of hot and cold material is the required driving force keeping the system far from equilibrium. On the basis of the stability analysis of the racemic final state, the results presented here demonstrate the existence of SMSB as a closed region (see Figs. 3, 5 and 6) in the phase representation of the reaction parameters. Explicit examples of SMSB are displayed in Figures 7 and 8 showing also the time dependence of the associated production of entropy for starting from two different initial concentrations.

The considerations given to the microreversibility condition in Secs I, II and III serve to underscore the fact that limited enantioselectivity-of and by itself– cannot lead to spontaneous mirror symmetry breaking, neither for a uniform temperature (i.e. at an experimental condition required to attain chemical equilibrium), not even for two temperatures (i.e. an experimental condition that excludes chemical equilibrium). By contrast, mirror symmetry breaking may be possible when in addition to a non-uniform temperature distribution the reactions (ii) and (iii) occur

in two distinct compartments held at different temperatures. The microreversibility arguments [8, 22], used as a proof of the correctness of the model, are necessary because we assume a scenario where chemical kinetics can be applied.

We briefly point out what modifications would have to be made in order to consider spatial temperature gradients. First, we need to input the temperature profile $T(x, y, z)$ as a known field. This converts the reaction rates k_i into spatially dependent functions via the Arrhenius relation. The kinetic rate equations must be replaced by partial differential reaction-diffusion-advection equations for the spatial and temporal dependence of the concentrations. The background convective flow of hot/cold material could be modeled by a steady hydrodynamical flow-field compatible with the compartment boundary conditions. In short, the technical complications would be considerable, but not insurmountable.

The significance of the above results with respect to applied absolute synthesis is somewhat limited due to the temperature difference required for achieving the essential inequality $k^*_{-3} > k_{-2}$. The point is, a sufficiently large difference would require high pressure conditions as well to maintain the media in a liquid state. By contrast, the results can be of significance in scenarios of prebiotic chemistry. In this context, the required experimental conditions of high temperature gradients and compartmentalization agree with those found in deep ocean hydrothermal vents, as we have previously reported [9]. Furthermore, the more relevant feature of this LES scenario is its ability to exhibit SMSB at very low reactant concentrations. In this respect, the detailed description given here for the effect on the SMSB dependence of the minimal internal flow rate -with respect to the compartment volumes at different temperatures- and on the reaction rate inequality $k^*_{-3} > k_{-2}$, shows that the variability range for SMSB of these parameters increases when the total system concentration C decreases, i.e. the probabilities for SMSB to occur *increase* in a prebiotic scenario. Notice that this overcomes the more important difficulty for a reasonable SMSB in a prebiotic scenario, where a specific prebiotic organic compound could be present, but only at very low concentrations. This, in spite of the presence of an important fraction of organic compounds, because of the diversity of different organic compounds in prebiotic scenarios [23]. While LES is ruled out as a scheme for SMSB in experimental conditions where thermodynamic equilibrium can be achieved, the results presented here open up the study for SMSB in scenarios of non-uniform temperature distributions, specific energy inputs to some species of the system, and compartmentalization, i.e. in conditions similar to those of living systems.

Acknowledgements

The research of CB and DH is supported in part by the Grant AYA2009-13920-C02-01, and that of JMR, JC, ZE-H and AM by AYA2009-13920-C02-02, from MICINN (currently MINECO).

Appendix A: Fluctuation equations

The linearized fluctuation equations that follow from the kinetic equations Eqs. (7-12) in Sec. II A are as follows. The overbar denotes a stationary solution of Eqs. (7-12).

$$\begin{aligned}\dot{\boldsymbol{\delta A}} &= \big(-2k_1-[k_2+k_3]\bar{\chi}-\frac{a}{V}-\frac{a}{V^*}\big)\boldsymbol{\delta A}+\Big(-(k_2+k_3)\bar{A}+(k_{-2}+k_{-3})\bar{\chi}+k_{-1}-\frac{a}{V^*}\Big)\boldsymbol{\delta\chi}\\ &+ (k_{-2}-k_{-3})\bar{y}\,\boldsymbol{\delta y}-\frac{a}{V}\boldsymbol{\delta\chi^*}\end{aligned} \tag{A1}$$

$$\dot{\boldsymbol{\delta\chi}} = (2k_1+[k_2+k_3]\bar{\chi})\boldsymbol{\delta A}+\Big((k_2+k_3)\bar{A}-k_{-1}-(k_{-2}+k_{-3})\bar{\chi}-\frac{a}{V}\Big)\boldsymbol{\delta\chi}+(k_{-3}-k_{-2})\bar{y}\,\boldsymbol{\delta y}+\frac{a}{V}\boldsymbol{\delta\chi^*} \tag{A2}$$

$$\dot{\boldsymbol{\delta y}} = (k_2-k_3)\bar{y}\boldsymbol{\delta A}-k_{-2}\bar{y}\boldsymbol{\delta\chi}+\Big(-k_{-1}-k_{-2}\bar{\chi}+(k_2-k_3)\bar{A}-\frac{a}{V}\Big)\boldsymbol{\delta y}+\frac{a}{V}\boldsymbol{\delta y^*} \tag{A3}$$

$$\begin{aligned}\dot{\boldsymbol{\delta\chi^*}} &= -\frac{V}{V^*}(2k_1^*+[k_2^*+k_3^*]\bar{\chi}^*)\boldsymbol{\delta A}+\Big(\frac{a}{V^*}-\frac{V}{V^*}(2k_1^*+[k_2^*+k_3^*]\bar{\chi}^*\Big)\boldsymbol{\delta\chi}\\ &+ \Big([k_2^*+k_3^*](\frac{C}{V^*}-\frac{V}{V^*}(\bar{A}+\bar{\chi})-\bar{\chi}^*)-k_{-1}^*-(k_{-2}^*+k_{-3}^*)\bar{\chi}^*-\frac{a}{V^*}-(2k_1^*+[k_2^*+k_3^*]\bar{\chi}^*)\Big)\boldsymbol{\delta\chi^*}\\ &+ (k_{-3}^*-k_{-2}^*)\bar{y}^*\,\boldsymbol{\delta y^*}\end{aligned} \tag{A4}$$

$$\dot{\boldsymbol{\delta y^*}} = -\frac{V}{V^*}\bar{y}^*(k_2^*-k_3^*)\boldsymbol{\delta A} - \frac{V}{V^*}\bar{y}^*(k_2^*-k_3^*)\boldsymbol{\delta\chi} + \frac{a}{V^*}\boldsymbol{\delta y} - (k_{-2}^*+k_2^*-k_3^*)\bar{y}^*\,\boldsymbol{\delta\chi^*} + \Big((k_2^*-k_3^*)(\frac{C}{V^*} - \frac{V}{V^*}(\bar{A}+\bar{\chi}) - \bar{\chi}^*) - k_{-1}^* - k_{-2}^*\bar{\chi}^* - \frac{a}{V^*}\Big)\boldsymbol{\delta y^*}. \quad \text{(A5)}$$

Specializing to the racemic fixed point $\bar{y} = \bar{y}^* = 0$ leads to the decoupling of the first three fluctuations from the latter two:

$$\dot{\boldsymbol{\delta A}} = \big(-2k_1 - [k_2+k_3]\bar{\chi} - \frac{a}{V} - \frac{a}{V^*}\big)\boldsymbol{\delta A} + \Big(-(k_2+k_3)\bar{A} + (k_{-2}+k_{-3})\bar{\chi} + k_{-1} - \frac{a}{V^*}\Big)\boldsymbol{\delta\chi} - \frac{a}{V}\boldsymbol{\delta\chi^*} \quad \text{(A6)}$$

$$\dot{\boldsymbol{\delta\chi}} = (2k_1 + [k_2+k_3]\bar{\chi})\boldsymbol{\delta A} + \Big((k_2+k_3)\bar{A} - k_{-1} - (k_{-2}+k_{-3})\bar{\chi} - \frac{a}{V}\Big)\boldsymbol{\delta\chi} + \frac{a}{V}\boldsymbol{\delta\chi^*} \quad \text{(A7)}$$

$$\dot{\boldsymbol{\delta y}} = +\Big(-k_{-1} - k_{-2}\bar{\chi} + (k_2-k_3)\bar{A} - \frac{a}{V}\Big)\boldsymbol{\delta y} + \frac{a}{V}\boldsymbol{\delta y^*} \quad \text{(A8)}$$

$$\dot{\boldsymbol{\delta\chi^*}} = -\frac{V}{V^*}(2k_1^* + [k_2^*+k_3^*]\bar{\chi}^*)\boldsymbol{\delta A} + \Big(\frac{a}{V^*} - \frac{V}{V^*}(2k_1^* + [k_2^*+k_3^*]\bar{\chi}^*\Big)\boldsymbol{\delta\chi} + \Big([k_2^*+k_3^*](\frac{C}{V^*} - \frac{V}{V^*}(\bar{A}+\bar{\chi}) - \bar{\chi}^*) - k_{-1}^* - (k_{-2}^*+k_{-3}^*)\bar{\chi}^* - \frac{a}{V^*} - (2k_1^* + [k_2^*+k_3^*]\bar{\chi}^*)\Big)\boldsymbol{\delta\chi^*} \quad \text{(A9)}$$

$$\dot{\boldsymbol{\delta y^*}} = +\frac{a}{V^*}\boldsymbol{\delta y} + \Big((k_2^*-k_3^*)(\frac{C}{V^*} - \frac{V}{V^*}(\bar{A}+\bar{\chi}) - \bar{\chi}^*) - k_{-1}^* - k_{-2}^*\bar{\chi}^* - \frac{a}{V^*}\Big)\boldsymbol{\delta y^*}, \quad \text{(A10)}$$

as reflected by the specific matrix entries in Eqs. (31,32).

Appendix B: Characteristic polynomial

The characteristic polynomial associated with the Jacobian matrix Eq. (29) evaluated at the racemic fixed point is

$$P(\lambda) = \det|J-\lambda I| = \det|A-\lambda I|\det|B-\lambda I|, = P^{(3)}(\lambda)P^{(2)}(\lambda), \quad \text{(B1)}$$

where I is the identity matrix and the quadratic and cubic polynomials are given by

$$P^{(2)}(\lambda) = \lambda^2 - \mathrm{tr}\big(B\big)\lambda + \det\big(B\big), \quad \text{(B2)}$$

$$P^{(3)}(\lambda) = -\lambda^3 + \mathrm{tr}\big(A\big)\lambda^2 + G\big(A\big)\lambda + \det\big(A\big), \quad \text{(B3)}$$

respectively, where

$$G\big(A\big) = -a_{11}a_{22} - a_{11}a_{33} - a_{22}a_{33} + a_{32}a_{23} + a_{12}a_{21} + a_{13}a_{31}. \quad \text{(B4)}$$

Thus, inserting Eqs. (B2,B3) into Eq. (B1), we obtain the fifth order polynomial

$$P(\lambda) = -\lambda^5 + [\mathrm{tr}\big(B\big) + \mathrm{tr}\big(A\big)]\lambda^4 + \{G\big(A\big) - \det\big(B\big) - \mathrm{tr}\big(B\big)\mathrm{tr}\big(A\big)\}\lambda^3 + \{\mathrm{tr}\big(A\big)\det\big(B\big) - G\big(A\big)\mathrm{tr}\big(B\big) + \det\big(A\big)\}\lambda^2 + \{G\big(A\big)\det\big(B\big) - \det\big(A\big)\mathrm{tr}\big(B\big)\}\lambda + \det\big(B\big)\det\big(A\big). \quad \text{(B5)}$$

[1] P. Cintas and C. Viedma, Chem. Commun. **47**, 12786 (2011).

[2] Z. El-Hachemi, J. Crusats, J. Ribó, J. McBride, and S. Veintemillas-Verdaguer, Angew. Chem. Int. Ed. **50**, 2359 (2011).
[3] W. Noorduin, T. Izumi, A. Millemaggi, M. Leeman, H. Meekes, W. van Enckevort, R. Kellogg, B. Kaptein, E. Vlieg, and D. Blackmond, J. Am. Chem. Soc. **130**, 1158 (2008).
[4] W. Noorduin, E. Vlieg, R. Kellogg, and B. Kaptein, Angew. Chem. Int. Ed. **48**, 9600 (2009).
[5] C. Viedma, Phys. Rev. Lett. **94**, 065504 (2005).
[6] J. Wattis, Orig. Life Evol. Biospher. **41**, 133 (2011).
[7] V. Avetisov and V. Goldanskii, Proc. Natl. Acad. Sci. USA **93**, 11435 (1996).
[8] J. Ribó and D. Hochberg, Phys. Lett. A **373**, 111 (2008).
[9] J. Ribó, J. Crusats, Z. El-Hachemi, A. Moyano, C. Blanco, and D. Hochberg, Astrobiology, accepted (AST-2012-0904.R1).
[10] J. Baross and S. Hoffman, Orig. Life Evol. Biosph. **15**, 327 (1985).
[11] N. Holm, Orig. Life Evol. Biosph. **22**, 5 (1992).
[12] W. Martin, J. Baross, D. Kelley, and M. Russell, Nature Rev. Microbiol. **6**, 805 (2008).
[13] S. Miller and J. Bada, Nature **334**, 609 (1988).
[14] J. Bernal, *The Physical Basis of Life* (Routledge, London, 1951).
[15] A. Brack, *Clay minerals and the origin of life, in Developments in Clay Science vol.1 Handbook of Clay Science* (Elsevier, Oxford, 2006).
[16] A. Cairns-Smith and H. Hartman, *Clay minerals and the origin of life* (Cambridge University Press, UK, 1986).
[17] J. Ferris, Elements **1**, 145 (2005).
[18] J. Ferris, Am. Mineralogist **91**, 1715 (2006).
[19] R. Chang, *Physical Chemistry* (University Science Books, Sausalito, 2000).
[20] J. Murray, *Mathematical Biology* (Springer, Sausalito, 1993), 2nd ed.
[21] D. Kondepudi and I. Prigogine, *Modern Thermodynamics: From heat engines to dissipative structures* (New York, Wiley, Sausalito, 1998), 2nd ed.
[22] D. Blackmond and O. Matar, J. Phys. Chem. B **112**, 5098 (2008).
[23] P. Schmitt-Kopplina, Z. Gabelicab, R. D. Gougeonc, A. Feketea, B. Kanawatia, M. Harira, I. Gebefuegia, G.Eckeld, and N. Hertkorna, Proc. Natl. Acad. Sci. USA **105**, 2763 (2010).

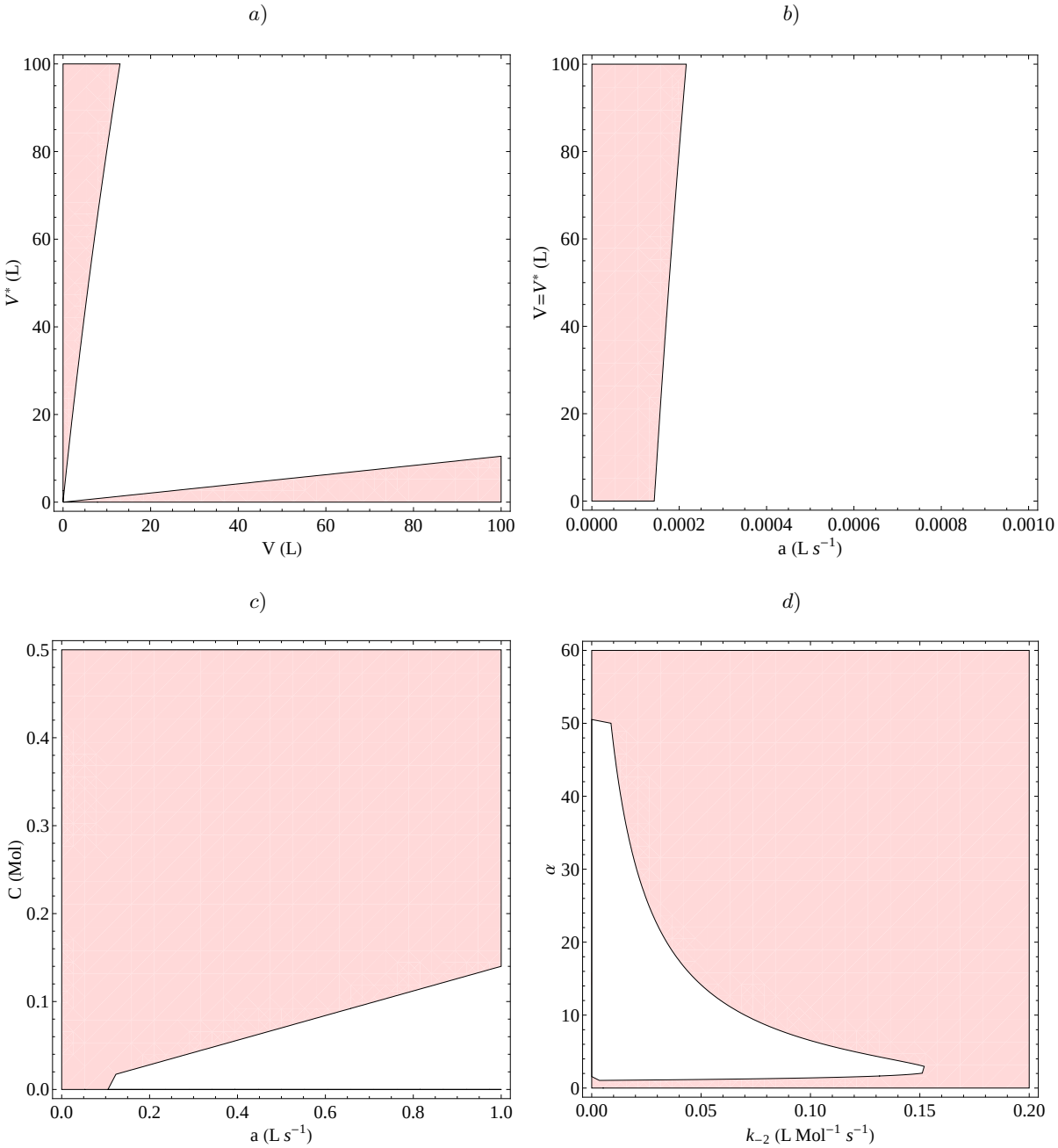

FIG. 2: White zones indicate where the racemic state is **unstable** to perturbations and so bifurcates to a chiral state (color/grayscale, where racemic state is stable) as a function of the indicated selected pairs of variables: a) The cold and hot compartment volumes V and V^*, b) the flow parameter a versus the volume of each compartment, holding $V = V^*$ fixed, c) the flow parameter a and the total system concentration C, and d) the reaction rate k_{-2} and α, where $\alpha = k^*_{-3}/k_{-2}$. Except for the specific pair that is varied in a),b),c), and d), the remainder of values are held fixed at $k_1 = 10^{-9}$, $k_{-1} = 10^{-15}$, $k_1^* = 10^{-7}$, $k_{-1}^* = 10^{-11}$, $k_2 = 10^2$, $k_{-2} = 10^{-4}$, $k_2^* = 0$, $k_{-2}^* = 0$, $k_3 = 0$, $k_{-3} = 0$, $k_3^* = 10^1$, $k_{-3}^* = 10^{-3}$, the volume and flux parameters $V = 10$, $V^* = 10$, $a = 0.1$. The initial concentrations $[A]_0 = 10^{-6}$, $[A^*]_0 = 10^{-6}$, $[L]_0 = 10^{-11}$, $[D]_0 = 10^{-11}$, $[L^*]_0 = 10^{-11} + 10^{-21}$, $[D^*]_0 = 10^{-11}$.

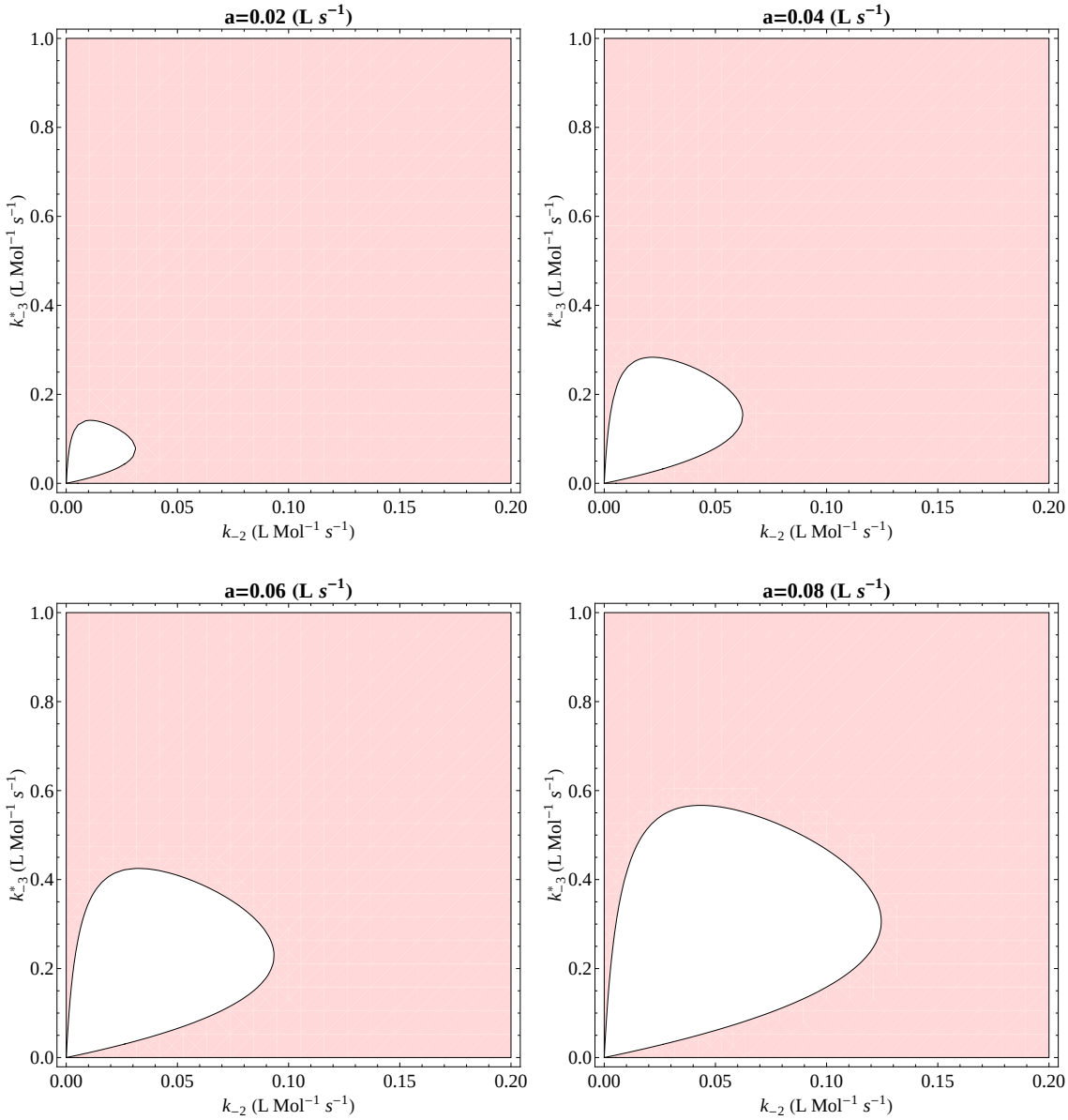

FIG. 3: White zones indicate where the racemic state is **unstable** to perturbations (color/grayscale, where its stable) for different values of k_{-2} and k^*_{-3}, and for different values of the internal flow parameter a. The area of the region of instability scales up with the flow rate. The remainder of parameters and initial concentrations as in Fig. 2.

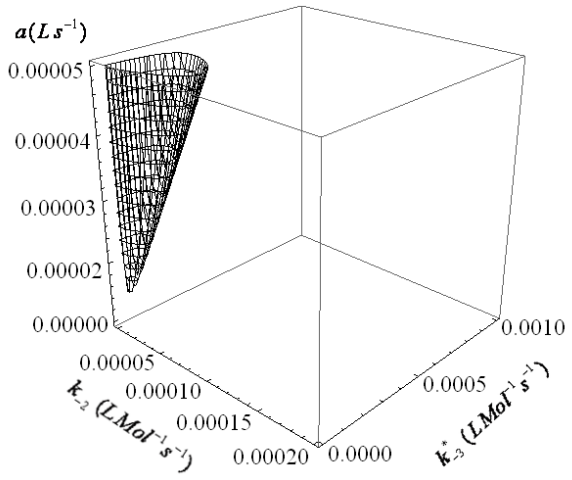

FIG. 4: Effect of varying the internal flow rate. Three dimensional figure represents all points for which the racemic state is **unstable** to perturbations. Increased flow enlarges the allowed region of instability. The racemic state is stable in the empty (white) domain. The remainder of parameters and initial concentrations as in Fig. 2.

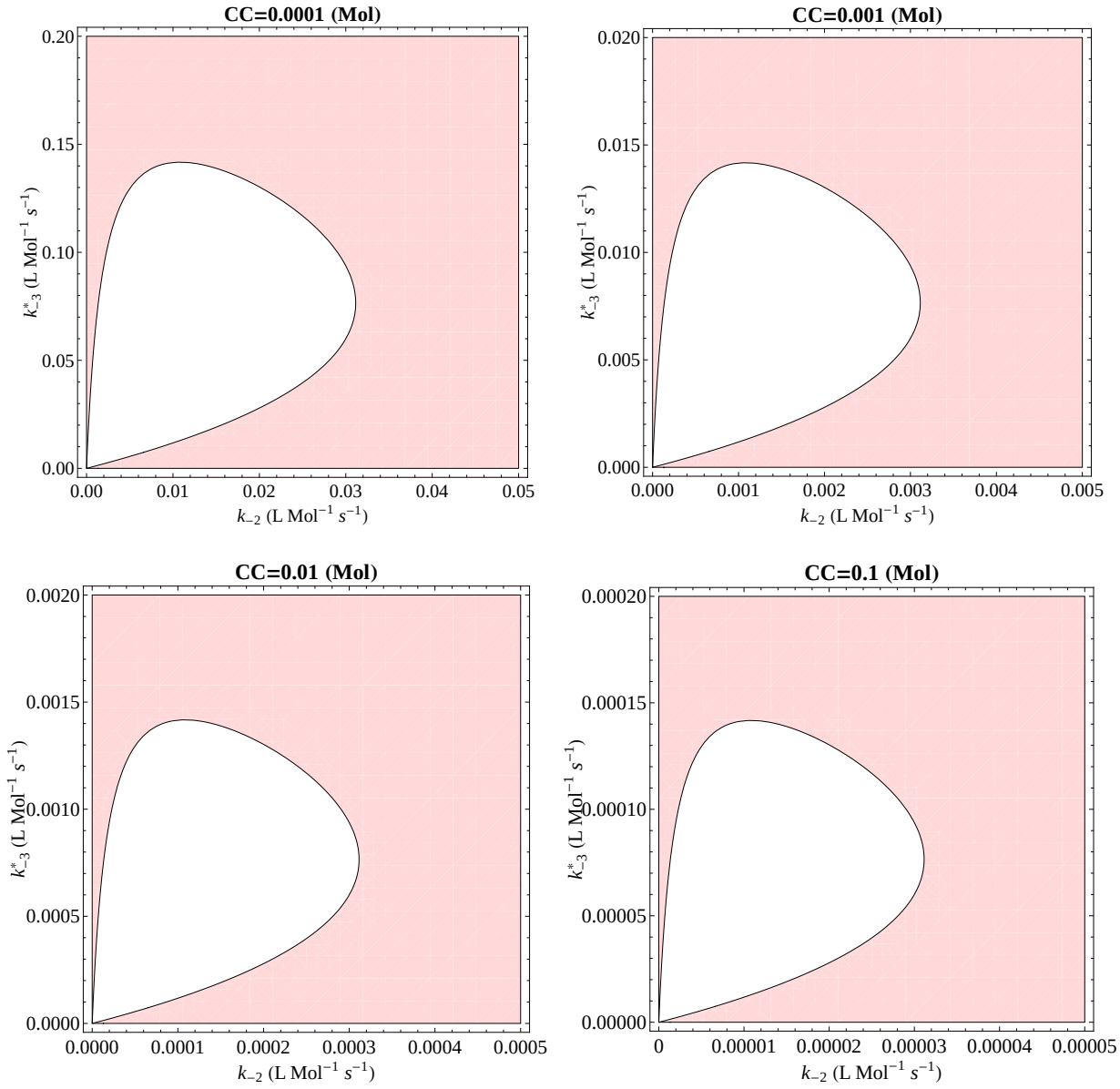

FIG. 5: Regions where the racemic state bifurcates to chiral states (in white) for different values of k_{-2} and k^*_{-3}, and for different values of the total concentration C. Increasing C decreases the ranges in both k_{-2} and k^*_{-3} for which the racemic state is linearly unstable. The remainder of parameters and initial concentrations as in Fig. 2.

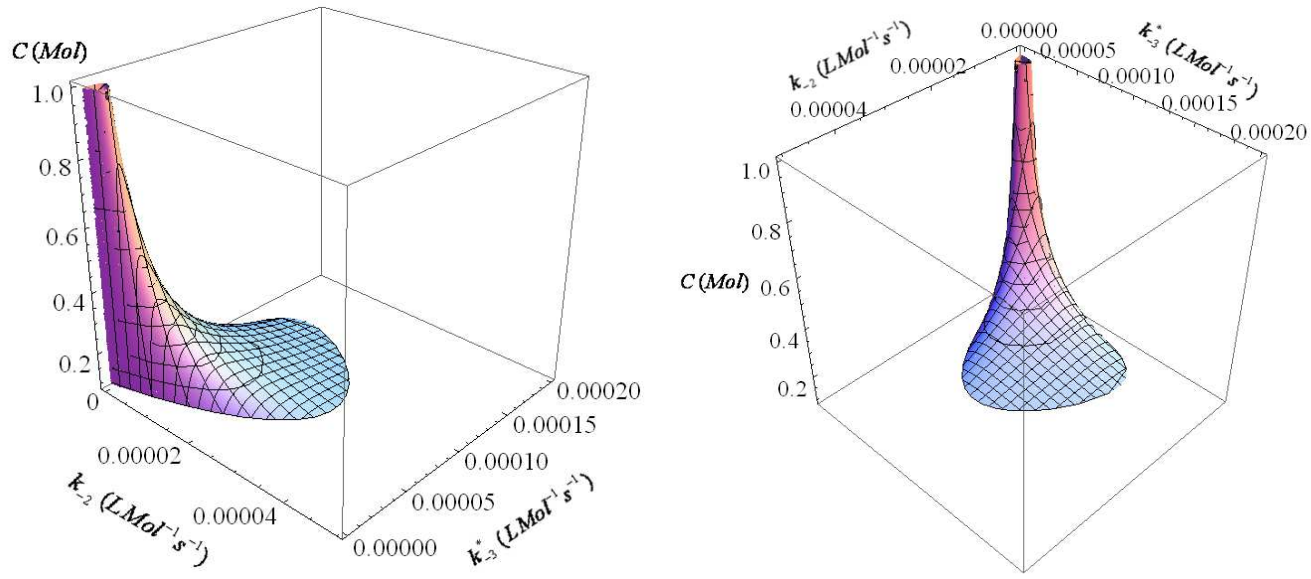

FIG. 6: Effect of varying the total system concentration C. The solid three-dimensional figure (color/gray) indicates where the racemic state is **unstable** to perturbations. Increasing the system concentration C *shrinks* the cross sectional domain k_{-2}, k^*_{-3} of instability. The racemic state is linearly stable in the empty (white) region. The remainder of parameters and initial concentrations are as listed in Fig. 2.

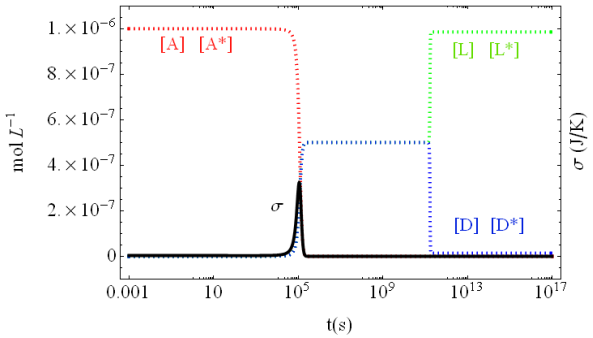

FIG. 7: Symmetry breaking bifurcation in the two compartment model, see Figure 1. For the rates and system parameters in given in Sec. IV B. The entropy production σ peaks at the onset of the induction period, well before the symmetry breaking bifurcation. Note $\sigma > 0$ for all times.

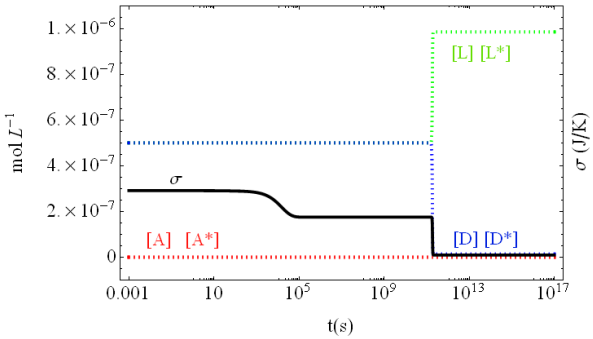

FIG. 8: Symmetry breaking bifurcation in the two compartment model, same rates and system parameters as in Figure 7. See text for the initial concentrations. In this case the entropy production σ (scaled up by a factor of 10^7) decreases monotonically and drops to a minimum (but nonzero) value at the symmetry breaking bifurcation, and remaining positive for all subsequent times.